Title

Formulation methods for peptide-modified lipid nanoparticles

Journal

Journal of Controlled Release, 385

ISSN

0168-3659

Authors

Miyasaki, Katelyn

Han, Sangwoo

Carton, Olivia

et al.

Publication Date

2025-09-01

DOI

10.1016/j.jconrel.2025.114030

HHS Public Access

Author manuscript

J Control Release. Author manuscript; available in PMC 2025 October 22.

Published in final edited form as:

J Control Release. 2025 September 10; 385: 114030. doi:10.1016/j.jconrel.2025.114030.

Formulation methods for peptide-modified lipid nanoparticles

Katelyn Miyasaki[a,*], **Sangwoo Han**[a,*], **Olivia Carton**[a], **Rebecca M. Kandell**[a], **Jonathan Gunn**[a], **Ester J. Kwon**[a]

[a]Department of Bioengineering, University of California, San Diego, La Jolla, CA, 92093, USA

Abstract

Lipid nanoparticles (LNPs) are a promising non-viral gene carrier, but one significant unmet challenge is cell-specific delivery in extrahepatic organs. Peptides are one class of targeting ligand that have been used to target nanoparticles, including LNPs. Herein, we compared two formulation approaches that use the polyethylene glycol (PEG)-lipid to display targeting peptides: (1) post-conjugation targeted (PCT), in which LNPs were formulated with PEG-lipid with chemical handles and subsequently modified with peptides, and (2) in-line targeted (ILT), in which peptide-PEG-lipid conjugates were directly used in LNP formulation. We observed that PCT and ILT LNPs had similar physicochemical properties, but ILT LNPs aggregated when formulated with a large peptide. Using cyclic RGD as a model ligand, we observed that while binding and uptake of LNPs in cultured cells were similar between approaches, PCT LNPs led to higher activity. Systemic administration revealed that LNPs formulated with both methods led to shifts in organ biodistribution compared to untargeted LNPs, but PCT resulted in higher transfection compared to ILT. Finally, analysis of cell tropism showed that the transfection activity of cRGD LNPs was shifted toward endothelial cells in multiple organs. We conclude that while PCT LNPs required more processing steps over the ILT LNPs, they led to superior formulations that led to active peptide targeting.

Keywords

LNP; mRNA; drug targeting; intravenous administration; peptides

INTRODUCTION

Lipid nanoparticles (LNPs) are currently the most clinically advanced non-viral gene therapy carrier.[1] Due to the flexibility of LNPs to carry a large diversity of nucleic acid payloads, including transiently-acting siRNA, miRNA, and mRNA as well as plasmid DNA and Cas9-guide RNA ribonucleoproteins, potential applications are abundant.[2–4] The first

Correspondence should be addressed to E.J.K. (ejkwon@ucsd.edu), 9500 Gilman Drive, La Jolla, CA 92093-0412.
*These authors contributed equally.

AUTHOR CONTRIBUTIONS

KM: Conceptualization, formal analysis, funding acquisition, investigation, methodology, writing — initial draft, and writing — review & editing. **SH:** Conceptualization, investigation, methodology, and writing — review & editing. **OC:** Conceptualization, investigation, and methodology. **JG:** Resources and writing — review & editing. **RK:** Investigation. **EJK:** Conceptualization, funding acquisition, methodology, project administration, resources, supervision, and writing — review & editing.

DECLARATION OF INTERESTS

The authors declare no competing interests.

LNP drug used in humans, Onpattro (patisiran), was approved by the FDA in 2018 for the systemic delivery of siRNA against transthyretin to treat hereditary amyloidosis.[5] It has been shown that the efficient gene transfer to hepatocytes is due to the adsorption of apolipoprotein E present in the blood onto the LNP surface, leading to engagement of LDL receptors.[6] There is an outstanding need to develop LNPs for cell specific delivery to extrahepatic organs.

The physicochemical properties of LNPs are known to have important roles in their pharmacokinetics and pharmacodynamics. For example, larger LNPs often have higher transfection, but are limited in their spread in tissues compared to smaller particles.[7,8] The Siegwart group has demonstrated that the addition of charged lipids into the LNP formulation can lead to what they have described as selective organ targeting (SORT), with significantly increased activity in the lungs or the spleen, noting that LNP pK_a correlated strongly with the organ biodistribution and transfection.[9,10] In addition to the passive targeting dictated by the physicochemical properties of nanoparticles that largely determines organ level biodistribution, nanoparticles can be modified with specific ligands to achieve active targeting. For example, LNPs have been targeted with antibodies to increase cargo delivery to T cells,[11,12] lymphatic endothelial cells,[13] and lung endothelial cells.[14] As an alternative to antibodies, peptides are potentially attractive ligands because they are relatively inexpensive to synthesize and are more stable, but can still represent a large diversity of bioactive binding motifs.[15] The low unimolecular affinity of peptides can be overcome by multivalent presentation on the nanoparticle surface.[16] Studies have demonstrated the use of peptide targeted LNPs to achieve cell tropism, including hematopoietic progenitor cells in the bone marrow,[17] photoreceptors in the eye,[18] hepatic stellate cells in the liver,[19] and cystic fibrosis lung epithelium.[20] As it stands, studies have used several different methods to produce peptide targeted LNPs, including incorporation of peptide-lipid conjugates fed directly into the formulation,[19–21] insertion of peptide-lipid conjugates after LNP formulation,[17,22] and peptide conjugation onto LNPs after formulation.[18]

Considering the importance of peptides as a class of targeting ligands, our goal was to compare two methods for the incorporation of peptides into LNP formulations: (1) post-conjugation targeted (PCT) formulation, in which we formulated LNPs with chemical handles on the PEG-lipid that were subsequently modified with peptide post-formulation, and (2) in-line targeted (ILT) formulation, in which we synthesized peptide-PEG-lipid conjugates that were directly used for LNP formulation (Fig. 1A). The PCT formulation requires more processing steps and therefore is more cumbersome and may introduce batch-to-batch variation in manufacturing; however, since peptides are reacted after LNP formulation, they are less likely to impact internal LNP structure and more likely to be displayed on the LNP surface for receptor engagement. Conversely, peptide incorporation in the ILT formulation can be done in a single formulation step and the peptide amount can be set by the input feed, offering a simple method for peptide-modified LNP manufacture. However, there is little control on the surface presentation of peptides. We did not consider the post-insertion method, as in our hands, the quantitative amount of peptide-lipid insertion was difficult to control. First, we compared the physicochemical properties of LNPs using five different peptides that represent various lengths and physicochemical properties and

observed both methods yielded LNPs with similar sizes, with the exception of the largest 31 amino acid peptide which led to aggregation of ILT formulated LNPs. Furthermore, we also observed greater size instability and lower yield for ILT LNPs. We then used cyclic RGD (cRGD) as a model peptide to compare LNP binding and transfection efficiency *in vitro* and LNP biodistribution and activity *in vivo*. While we observed similar LNP binding and uptake between the two conjugation methods, PCT LNPs mediated a two-fold greater expression of cargo mRNA compared to ILT LNPs. After systemic administration *in vivo*, we observed that both PCT and ILT LNPs led to changes in biodistribution and activity compared to untargeted LNPs. Most notably, cRGD targeting led to elevation of expression in the lungs and spleen and decreased expression in the liver compared to untargeted LNPs. We delivered mRNA encoding Cre recombinase in Ai9 mice to observe a cell tropism shift towards endothelial cells with cRGD targeting. Our results indicate that post-modification of LNPs with targeting peptides leads to more controlled LNP size and improved transfection efficiency while altering organ and cell-level tropism of LNPs.

RESULTS

Characterization of in-line and post-conjugation peptide LNPs

Peptides chosen for conjugation include linear RGD, cyclic RGD, CGKRK, VCAM-1, and RVG. These peptides represented a range of lengths from 4–31 residues (Table 1). Linear and circular peptides with the motif “RGD” are frequently used to target cancer cells that overexpress integrins.[23] CGKRK is a peptide identified by phage display known to bind to tumor stroma and neovasculature.[24] VCAM-1 peptide was also identified by phage display[25] and binds to upregulated VCAM-1 on inflamed endothelium.[26,27] RVG is a peptide from rabies virus glycoprotein used to target neurons.[28,29] Peptides were synthesized with a cysteine for conjugation chemistry and a carboxyfluorescein (FAM) label. For ILT LNPs, PEG-lipid conjugates were prepared through reaction of DSPE-PEG-maleimide and cysteine-bearing peptides and purification by size exclusion chromatography. PEG-lipid peptide conjugates were dissolved in ethanol and were fully soluble prior to formulation. In order to formulate PCT and ILT LNPs, we used as a base the Onpattro formulation with a lipid composition of 50:10:38.5:1.5 of DLin-MC3-DMA:DSPC:cholesterol:PEG-lipid (Fig. S1).[4,30] Of the 1.5 mole% PEG-lipid, we used 1 mole% DMG-PEG. The remaining 0.5 mole% was composed of DSPE-PEG-maleimide for PCT LNPs and 0.35 mole% DSPE-PEG-maleimide and 0.15 mole% DSPE-PEG-peptide conjugate for ILT LNPs (Fig. 1A). LNPs were formulated at a lipid/RNA mass ratio of 20.7 using polycytidylic acid (polyC) RNA using a microfluidic staggered herringbone mixer, as described previously.[31,32] An additional 0.6 mole% of the lipophilic dye 1,1’-Dioctadecyl-3,3,3’,3’-Tetramethylindocarbocyanine Perchlorate (DiI) was included to label LNPs and approximate yield. For PCT LNPs, formulations were reacted with 0.15 mole% of peptide for 2 hours and free peptides were purified via diafiltration.

We compared physicochemical properties (hydrodynamic diameter, polydispersity, zeta potential) of LNPs (Fig. 1B–D). For most peptides, PCT and ILT formulated LNPs resulted in LNPs of similar size, although the ILT LNPs yielded slightly larger nanoparticles with higher polydispersity indices (Fig. 1B–C). ILT formulation was unsuitable for larger

peptides; there was clear aggregation of RVG ILT LNPs, possibly due to the larger peptide causing destabilization of the LNP structure. As expected, zeta potential measurements corresponded between formulations for a given peptide (Fig. 1D), indicating that changes in surface potential measurements were likely due to peptide modification. We measured the ratios of peptide/LNP, peptide yield, and LNP yield through absorbance measurements of FAM-labeled peptides and DiI, with the assumption that DiI was representative of the total RNA content of our formulation (Fig. 1E–G). Using DiI as a proxy for lipid content in LNPs is supported by a previous study that showed that theoretical N/P closely matched measured N/P ratios, indicating that DiI should be proportional to the RNA content.[33] The peptide/LNP ratios were similar across different peptides, indicating successful incorporation of peptides at similar quantities for both methods. While volumes and processing steps varied between PCT and ILT LNPs, total DiI yields were similar across formulations with the exception of ILT RVG LNPs that showed aggregation by DLS (Fig. 1B). Total yields of peptide were more varied (Fig. 1G), indicating potential peptide-specific differences in reaction efficiency for PCT LNPs or incorporation efficiency for ILT LNPs. LNP size remained stable for all formulations over 1 week of storage at 4 °C (Fig. S2).

In vitro transfection efficiency, binding, and uptake

Active targeting was evaluated between both formulation methods using the peptide cyclic RGD (cRGD). We chose cRGD as a model peptide to demonstrate peptide-mediated LNP targeting due to the wealth of existing studies that have established the specificity of RGD targeting on nanoparticles, knowledge of its receptors, and the availability of established *in vitro* and in vivo models.[23] The RGD motif is known to bind a number of integrin receptors, most notably $\alpha_V\beta_3$, $\alpha_V\beta_5$, and $\alpha_5\beta_1$, that have upregulated expression in many physiological settings including inflammation and cancer, but also may be expressed at low levels in healthy tissues.[23,34–37] We selected cRGD because it is known to more stably bind than linear RGD;[38,39] one study showed a thousand-fold lower IC_{50} for cyclized RGD compared to linear RGD for platelet aggregation.[40]

We investigated whether cRGD targeting would mediate increased transfection activity of LNPs. First, we determined the physicochemical properties of LNPs formulated with different amounts of cRGD. After formulation of LNPs with 1 mole% DSPE-PEG-maleimide, we split the batch into 4 parts and titrated cRGD at 0, 0.17, 0.3, and 0.5 mole%. These levels of peptide modification were selected based on previous peptide-targeted LNP studies. The Sahay group observed effective transfection in the retina at 0.15 and 0.3 mole% peptide, and the Heidenreich group observed increased LNP accumulation in the bone marrow with 0.1 mole% peptide.[17,18] The Mitchell group used 0.15 mole% in targeting LNPs to the brain.[41] One group used 2% peptide-PEG-lipid, but with 5 mole% total PEG-lipid compared to our 1.5 mole% PEG-lipid.[19] cRGD LNPs at all mole% had similar sizes and PDIs (Fig. 2A–B). Zeta potential decreased with increasing cRGD mole% (Fig. 2C), indicating increasing cRGD surface modification. The amount of peptide conjugated was estimated, as in Fig. 1E, via the absorbances of FAM and DiI, and increased mole% of peptide led to higher peptide to LNP ratios (Fig. 2D). LNP activity was evaluated in MDA-MB-435 cells (Fig. 2E), a human cancer cell line that highly expresses $\alpha_V\beta_3$ integrin.[42] We observed increases in transfection efficiency with increasing peptide amounts, up to

21-fold over untargeted with 0.5 mole% cRGD. When we performed a similar study with linear RGD, we did not observe improvements in transfection efficiency with increasing peptide amounts (Fig. S3), consistent with the increased binding affinity of cRGD over RGD reported by others.[38,39]

Since 0.5 mole% cRGD PCT LNPs exhibited the highest transfection, we next compared PCT and ILT LNPs with 0.5 mole% of cRGD. PCT LNPs were formulated with 1 mole% DMG-PEG and 0.5 mole% DSPE-PEG-maleimide, then reacted with cRGD at a 1.2-fold excess. ILT LNPs were formulated with 0.5 mole% DSPE-PEG-cRGD. LNPs were formulated with FLuc mRNA and DiI to visualize particles. The properties of cRGD LNPs formulated with FLuc mRNA and 0.5 mole% cRGD (Fig. 2A–D) were similar to nanoparticles formulated with polyC (Fig. 1B–E, Fig. S4A–D). We observed that cRGD LNP properties were generally consistent across experiments, including formulations with different nucleic acid cargo and diafiltration steps. However, we also observed that at 0.5% peptide, some formulations of ILT LNPs had a greater propensity to aggregate over untargeted or PCT LNPs when stored at 4 °C (Fig. S4E). We also observed a significant loss of RNA yield in ILT LNPs compared to PCT LNPs at 0.5 mole% peptide (Fig. S4F). Despite similar physicochemical properties (Fig. 1), PCT LNPs mediated more than double the expression over ILT LNPs, which showed similar expression compared to untargeted LNPs (Fig. 2F).

In order to understand the increased transfection efficiency of PCT LNPs over ILT LNPs, we investigated LNP binding and uptake with the same 0.5 mole% cRGD LNPs. We first evaluated binding by incubating LNPs with cells at 4 °C to halt energy dependent internalization. DiI-labeled LNPs were incubated with MDA-MB-435 cells at 4 °C for 3 hours and cells were imaged via fluorescence microscopy. We observed relatively low binding of untargeted LNPs and image quantification revealed an 8- to 12-fold increase in binding when both PCT and ILT LNPs were targeted with cRGD (Fig. 3A–B). We also performed this study with analysis by flow cytometry to quantitate association on a per cell basis and observed similar results (Fig. 3C). After confirming similar degrees of binding to cells at 4 °C, we compared binding and uptake at 37 °C with flow cytometry (Fig. 3D). Uptake of all LNPs increased between 15 min and 30 min and plateaued at 60 min, and uptake was greater for both cRGD PCT and ILT LNPs compared to untargeted LNPs. A similar trend was observed when measuring uptake via the FITC-labeled cRGD peptides (Fig. 3E). We concluded that cRGD modification increases LNP binding and uptake in cells regardless of the formulation method.

We then performed competitive binding assays with free cRGD to confirm that the increase in LNP binding and transfection we observed with cRGD targeting was receptor specific. We preincubated MDA-MB-435 cells with free cRGD or equivalent amounts of DMF vehicle at 4 °C and analyzed the binding of cRGD LNPs made with 0.15 mole% peptide at 4 °C for 1 hour. In analysis through imaging,[43] we observed that cRGD LNPs binding was significantly reduced in the presence of free cRGD (Fig. 4A–B). With 0.15 mole% cRGD and after 24 hours, PCT and ILT cRGD LNPs both exhibited increased transfection compared to untargeted LNPs in MDA-MB-435 cells (Fig. 4C). Similar to binding studies, we observed significant reduction of transfection activity in the presence of free cRGD in

a dose-dependent manner for both PCT and ILT cRGD LNPs (Fig. 4D). Minimal change was observed in the transfection efficiency of untargeted LNPs. In human umbilical vein endothelial cells (HUVECs), we also observed cRGD-dependent transfection of LNPs that could be competed with free cRGD in a dose-dependent manner, indicating cRGD targeting was relevant for multiple cell types (Fig. 4E–F).

We next evaluated LNP pharmacokinetics and activity *in vivo*. LNPs at 0.5 mole% cRGD were formulated with the near-infrared lipophilic dye 1,1'-Dioctadecyl-3,3,3',3'-Tetramethylindotricarbocyanine Iodide (DiR) to aid *in vivo* imaging. LNP physicochemical properties were similar to previous cRGD formulations (Fig. S5). LNPs were injected intravenously via the tail-vein and blood was collected over 4 hours and organs collected at 6 hours (Fig. 5A). Blood half-lives of LNPs were calculated based on a one phase exponential decay[44] and we observed that the addition of targeting ligand decreased the blood half-life of LNPs from 41.8 min for untargeted LNPs to 10.5 min for PCT and 12 min for ILT LNPs (Fig. 5B). Our measured half-life was similar to previous reports of RGD-targeted liposomes, which decreased in blood half-life from ~102 min to ~9–10 min when the mole% of RGD was increased from 0.1 mole% to 1 mole%.[45] In analysis of organ biodistribution, targeted LNPs showed a near order of magnitude greater accumulation in the lungs and spleen and a modestly decreased accumulation in the heart and kidney compared to untargeted LNPs (Fig. 5C–D). Untargeted LNPs had highest accumulation in the liver whereas cRGD targeted LNPs had highest accumulation in the spleen. Both PCT and ILT targeted LNPs displayed similar biodistribution.

We evaluated expression mediated by cRGD targeted LNPs through measurement of luciferase activity in homogenized organs. Expression in organs predominantly followed biodistribution results, with cRGD targeted LNPs displaying significantly increased expression in the lungs and spleen and decreased expression in the heart compared to untargeted LNPs (Fig. 5E). Conversely, despite unobservable differences in liver accumulation, liver expression was significantly decreased with cRGD targeting 6- to 8-fold.

Considering PCT formulated LNPs could achieve greater *in vitro* (Fig. 2F) and *in vivo* activity (Fig. 4E), as well as more uniform and stable nanoparticles with higher yields, we considered it a superior formulation over ILT formulated LNPs. Lastly, we investigated cell tropism mediated by the cRGD ligand using the PCT formulation method. LNPs were formulated with mRNA encoding Cre recombinase and administered systemically into Ai9 mice (n=3). The cells of Ai9 mice express robust tdTomato protein when exposed to Cre recombinase,[46] allowing us to observe the cell tropism of the LNPs. We analyzed organs by histology 1 week after LNP administration and selected representative images (Fig. 6A). We observed that cRGD targeting increased reporter tdTomato expression in endothelial cells in the heart and lungs (Fig. 6B–C), and decreased expression in cardiomyocytes in the heart (Fig. 6B). Quantification of tdTomato expression in whole organ slices using QuPath image analysis software revealed a modest decrease in the number of transfected cells in the heart and a ~20-fold increase in CD31 positive cells when LNPs were targeted with cRGD (Fig. 6D). In the lung, where the number of cells transfected by untargeted LNPs was low, there was an 8-fold increase in the number of tdTomato expressing cells/mm^2 that were 93% CD31 positive after cRGD LNP administration (Fig. 6E). This shift away

from cardiomyocytes towards endothelial cells may be the cause of decreased transfection efficiency observed in the heart (Fig. 5E). On the other hand, the increase in endothelial expression in the lungs likely accounts for the increase in transfection efficiency. The robust tdTomato expression observed in the spleen appears to be in endothelial cells and macrophages, although we were unable to confirm the specific cell types. The amount of tdTomato signal was lower in the liver overall, consistent with the organ-level luciferase expression. These results are corroborated by whole-organ scans of each non-brain organ (Fig. S6–7).

DISCUSSION

Since the first FDA approvals of LNPs to treat liver disease and mRNA vaccines, there are numerous LNPs under clinical development. Targeted delivery to specific cell types would further broaden the scope of applications and greater on-target delivery would expand the therapeutic index. While several studies have examined the use of peptide targeted LNPs to improve tissue and cell specificity, no study has examined how different peptide conjugation methods may affect LNP properties or function. In our study, we compared formulation methods to incorporate peptide ligands through an in-line process using pre-conjugated peptide-lipids or in a post-conjugation process after formation of nanoparticles. We showed that while both methods for peptide incorporation into LNPs can yield nanoparticles with similar physicochemical properties and association in cells and organs, the method of peptide incorporation significantly impacted LNP functionality. Despite the advantages of increased simplicity and control of the in-line formulation process that make it appealing for manufacturing, post-conjugation was found to be a superior process for formulating peptide targeted LNPs because it was compatible with a larger diversity of peptides, formed more stable nanoparticles with higher yields, and led to LNPs with higher activity *in vitro* and *in vivo*.

We chose cRGD as a model ligand because it has been highly characterized as a targeting ligand in other nanoparticle platforms, allowing us to compare between studies. We observed elevations of cRGD-targeted LNPs in the spleen and lungs (Fig. 5D), consistent with the known expression of integrin αvβ3 in lung vasculature and on spleen mononuclear cells across multiple species.[47] This result was somewhat consistent with studies of RGD-targeted liposomes, which have elevated accumulation in the spleen and liver.[45,48] It is also known that RGD can bind to many other integrins in addition to αvβ3, including αvβ4, αvβ5, α5β1, αvβ6,[36,37] which may explain cRGD LNP transfection of healthy cells. We observed targeting decreased LNP blood half-life. The ~3- to 4-fold decrease in blood half-life of cRGD-targeted LNPs over untargeted LNPs (Fig. 5B) is likely due to the increased accumulation in the spleen and lungs. Similarly, cyclic RGD-targeted liposomes also had decreased blood half-life and an increased accumulation in spleen and liver.[45] Furthermore, the method in which targeting peptides were incorporated impacted functionality. We hypothesize that PCT LNPs yielded higher activity compared to ILT LNPs despite similar cell and organ association because peptides were only displayed on the surface of the LNP, allowing for engagement of receptors but minimally impacting LNP formation. The internal structure of LNPs has been shown to influence LNP transfection efficiency, for example by modifying the stability of the mRNA cargo inside bleb structures.[49] In another

study, linear RGD was incorporated into LNPs through covalent attachment to the ionizable lipid.[21] While these RGD-LNPs carrying luciferase mRNA displayed an approximately 5- to 6-fold greater whole-body luminescence signal in live mice compared to an untargeted control, the source of elevated transgene expression was undetermined; livers and spleens were measured and neither appeared to be driving the elevated expression.

One challenge in studying LNP targeting is that biodistribution and activity are not perfectly correlated.[8] For example, one study modeled the pharmacokinetic and pharmacodynamics of mRNA LNPs and separately characterized uptake and expression, observing that post-inserting an IgG-PEG-lipid into LNPs reduced liver accumulation by ~2-fold in the liver, but reduced expression by ~7-fold.[50] We observed a similar shift with our cRGD-targeted LNPs, which had similar accumulation in liver to untargeted LNPs but significantly less transgene expression (Fig. 5D–E). The non-linear correlation between biodistribution and activity was also observed in SORT LNPs, which achieve organ-specific accumulation driven by LNP pK_a and the resulting serum protein interactions.[9] Peptide conjugation influences both physicochemical properties like pK_a and interactions with specific targets on cell surfaces, and therefore receptor-ligand interactions may not be independent of global changes in biodistribution. Nonetheless, cRGD targeting was clearly able to shift the cellular tropism of LNP-mediated transgene expression to endothelial cells in multiple organs after systemic delivery, supporting the use of peptide ligands for LNP active targeting.

CONCLUSION

While our study clearly demonstrated advantages of PCT formulation over ILT formulation, what remains to be understood is the specific mechanism for the differences in transfection efficiency. Further work could delineate whether peptide modification impacts LNP structure and/or protein corona formation. Also, it is likely that each peptide ligand requires individual optimization of parameters such as conjugation density and linker length due to unique ligand-receptor interactions and impact of peptide conjugation on physicochemical properties of the LNP as a whole. Future studies could also investigate a diversity of PEG-lipids used to anchor peptides to the LNP surface, including the length and saturation of the lipid anchor, length and structure of the PEG, and degradability.

MATERIALS AND METHODS

In vitro transcription of RNA

DNA templates for generating FLuc mRNA were linearized with XhoI from plasmids received from the Mali Lab at UC San Diego. DNA templates were purified using the PureLink PCR purification kit (Invitrogen). RNA products were then produced using the HiScribe T7 RNA Synthesis Kit (NEB), with the addition of supplemental ATP (TriLink) and CleanCap Reagent AG (TriLink). Furthermore, N1-methylpseudouridine (TriLink) was substituted for UTP. RNA products were treated with DNAse I (NEB) and purified via the Monarch RNA Cleanup Kit (NEB). IVT mRNA was quantified via NanoDrop.

Synthesis of DSPE-PEG-peptides

Peptides were acquired from Lifetein (RGD, CGKRK, VCAM1) and CPC (cRGD, RVG). DSPE-PEG-Mal, MW 3.4k dissolved in PBS was reacted with peptides dissolved in dimethylformamide for 2 hr at RT. RVG was reacted with DSPE-PEG-Mal in dimethylformamide with additional 50 mM TEA. Conjugates were then purified via PD10 column and lyophilized. DSPE-PEG-RVG was additionally purified on an ENrich SEC 70 10 × 300 column (Bio-Rad). DSPE-PEG-peptides were reconstituted in ethanol and their concentrations measured via absorbance of the FAM label (Genesis UV-Visible Spectrophotometer). All DSPE-PEG-peptide conjugates appeared fully soluble in ethanol.

LNP formulation

(6*Z*,9*Z*,28*Z*,31*Z*)-heptatriaconta-6,9,28,31-tetraen-19-yl-4-(dimethylamino) butanoate (DLin-MC3-DMA) was purchased from BioFine International Inc. 1,2-distearoyl-*sn-glycero*-3-phosphocholine (DSPC), 1,2-dimyristoyl-*rac-glycero*-3-methoxypolyethylene glycol-2000 (DMG-PEG-2000), and cholesterol were purchased from Avanti Polar Lipids. DSPE-PEG-Maleimide, MW 3.4k was purchased from Laysan Bio. 1,1′-Dioctadecyl-3,3,3′,3′-tetramethylindocarbocyanine perchlorate (DiI) was purchased from Sigma Aldrich and 1,1'-Dioctadecyl-3,3,3',3'-tetramethylindotricarbocyanine iodide (DiR) was purchased from ThermoFisher.

All mRNA LNPs were formulated with DLin-MC3-DMA : DSPC : cholesterol : PEG-lipid at a mole ratio of 50 : 10 : 38.5 : 1.5 and weight ratio of 20.7 lipids/RNA (N/P of ~5.6). To prepare LNPs, lipids in ethanol and oligonucleotides in 25 mM acetate buffer, pH 4.0 were combined at a flow rate of 1 : 3 in a PDMS staggered herringbone mixer.[31,32] Lipophilic dyes in DMSO were also included in the lipid-ethanol mixture. Mixer channels were 200 by 100 μm, with herringbone structures 30 μm high and 50 μm wide. Immediately after formulation, 3-fold volume of PBS was added and LNPs were purified in 100 kDa MWCO centrifugal filters to less than 0.5% ethanol. Peptides in dimethylformamide were added to PCT LNPs with maleimide and reacted at RT for 2 hours, after which the reaction was quenched with free L-cysteine (Sigma). Free peptide was purified from PCT LNPs via Microcon 30 kDa centrifugal filters (Millipore Sigma) or Nanosep 300 kDa centrifugal filters (Pall). LNPs were stored in PBS at 4 °C for up to 1 month. LNP hydrodynamic diameter, polydispersity index, and zeta potential were measured by dynamic light scattering (Malvern NanoZS Zetasizer) in PBS. The RNA content and percent encapsulation were measured with and without Triton X-100 using a Quant-it RiboGreen RNA Assay (Invitrogen) according to the manufacturer's protocol. Peptide quantification was measured via absorbance (Genesis UV-Visible Spectrophotometer).

For the comparison of physicochemical properties of PCT and ILT LNPs, polycytidylic acid potassium salt (Sigma) was used as a substitute for mRNA. PCT LNPs were formulated with 1% DMG-PEG and 0.5% DSPE-PEG-maleimide (MW 3.4k) and reacted with 0.15 mole% peptide. ILT LNPs were formulated with 1% DMG-PEG, 0.35% DSPE-PEG-malemide, and 0.15% DSPE-PEG-peptide. Free peptide was purified from PCT LNPs in 30 kDa MWCO centrifugal filters.

For *in vitro* binding, uptake, and transfection studies, LNPs were purified in either 30 or 100 kDa MWCO centrifugal filters.

For *in vivo* blood half-life, biodistribution, and transfection studies, DiR was added to LNPs at 1 mol% and LNPs were sterile filtered in a 0.22 μm syringe filter. DiR absorbance was measured via a NanoQuant plate on a Tecan Spark plate reader.

LNP activity *in vitro*

MDA-MB-435 cells (ATCC) were cultured in Dulbecco's modified Eagle's medium (Corning) supplemented with 10% fetal bovine serum (GeminiBio). HUVECs (ATCC) were cultured in EGM-2 (Lonza). For characterizing *in vitro* transfection efficiency, cells were plated at 25,000 cells per cm^2 in 96-well plates to reach ~30% confluency 24 hours later. LNPs formulated with FLuc mRNA at 0.1 and 0.05 μg mL^{-1} in PBS were added to cells in volumes not exceeding 10% of the media volume. After an additional 72 hours of culture time, cells were lysed with Cell Culture Lysis Reagent (Promega) and luciferase expression in the lysates quantified with the Luciferase Assay System (Promega).

For competition studies, MDA-MB-435 cells were plated at 37,500 cells per cm^2 and HUVECs were plated at 17,500 cells per cm^2 in 96-well plates. MDA-MB-435 cells reached ~30–40% confluency and HUVECs reached ~70–80% confluency at the time of transfection 24 hours later. Free cRGD dissolved in DMF and PBS or an equivalent concentration of DMF in PBS were added to cells and incubated for 1 hr. Cells were then treated with LNPs at 100 ng/well, cultured for an additional 24 hours, then lysed with Cell Culture Lysis Reagent (Promega) and luciferase expression in the lysates quantified with the Luciferase Assay System (Promega).

LNP binding and uptake *in vitro*

MDA-MB-435 cells were cultured to 70–90% confluency before use in binding and uptake experiments. For binding and imaging, cells were plated at 42,000 cells per cm^2 in 24 well plates on glass coverslips treated with 0.05 mg mL^{-1} poly-D-lysine for 1 hr at 37°C. Cells were washed once with cold OptiMEM serum-free media, then incubated with LNPs at ~360 ng mRNA per well in OptiMEM. LNPs were dosed by DiI, thus the mRNA dose varied slightly. LNPs were placed on a rocker at 4 °C for 3 hrs. LNPs were then washed 3x with PBS and fixed for 10 min at RT in 4% paraformaldehyde. Images were obtained on a Nikon Eclipse Ti2 (Nikon Instruments Inc.) at 20x magnification and analyzed in Fiji.[51]

For cRGD binding competition studies, cells were plated at 50,000 cells per cm^2 in a glass-bottomed 96-well plate treated with 0.1 mg mL^{-1} poly-D-lysine for 1 hr at 37°C. Cells were washed once with cold OptiMEM, preincubated with free cRGD for 0.5 hr, then incubated with LNPs at ~100 ng mRNA per well at 4 °C for 1 hrs. LNPs were then washed 3x with PBS and fixed for 10 min at RT in 4% paraformaldehyde. Images were obtained on a Nikon Eclipse Ti2 (Nikon Instruments Inc.) at 20x magnification and analyzed in Fiji[51] and QuPath[43].

For binding measured by flow cytometry, cells were plated at 50,000 cells per cm^2 in a 96-well plate. Cells were washed once with cold OptiMEM serum-free media, then incubated

with LNPs at ~60 ng mRNA per well. LNPs were dosed by DiI, thus the mRNA dose varied slightly. LNPs were placed on a rocker at 4 °C for 3 hrs. Cells were then washed 3x in cold PBS and trypsinized. Samples were then combined (two wells for each sample) in a 96-well U-bottom plate, pelleted, and resuspended in staining buffer (2% FBS + 0.5 mM EDTA in PBS) with Sytox Blue live/dead stain (Invitrogen). Cells were analyzed on a NovoCyte flow cytometer (Agilent).

For uptake, cells were plated at 50,000 cells per cm^2 in a 96-well plate. LNPs at ~60 ng mRNA per well was added to cells via media change. LNPs were dosed by DiI. LNPs were incubated at 37 °C for 15, 30, or 60 min. Cells were then washed 3x in PBS and trypsinized. Samples were then combined (two wells for each sample) in a 96-well U-bottom plate, pelleted, and resuspended in staining buffer (2% FBS + 0.5 mM EDTA in PBS) with Sytox Blue live/dead stain (Invitrogen). Cells were analyzed on a NovoCyte flow cytometer (Agilent).

Pharmacokinetics and expression of LNPs after systemic administration

All animal experiments were performed in accordance with the University of California's Policy on the Use of Animals in Research and Teaching and are approved by the University of California San Diego Institutional Animal Care and Use Committee (IACUC), PHS Assurance Number D16-00020. LNPs formulated with 1% DiR were injected via the tail vein in 8-week-old female C57BL/6J mice (Jackson Labs 000664) and allowed to circulate for 6 hours. Blood was collected from the tail at 5, 15, 30, 60, 90, 120, 180, and 240 minutes for blood half-life analysis. Six hours post-administration, mice were perfused with PBS and organs were harvested for imaging analysis. Fluorescent signal from DiR-labeled LNPs in blood and organ samples was imaged with a LiCor Odyssey fluorescence scanner and quantified in ImageJ. Harvested organs were lysed through 3 freeze/thaw cycles and homogenized with a Tissue-Tearor handheld homogenizer Reporter Lysis Buffer (Promega) until homogeneous. Supernatants of homogenates were measured with a Luciferase Assay System (Promega) following manufacturer protocols. Protein content of supernatants was determined with a BCA assay following standard protocols. Statistical analysis was performed in GraphPad Prism.

Cellular tropism of LNPs after systemic administration

UT and PCT cRGD LNPs were formulated with Cre mRNA and injected via the tail vein in 11-week-old female Ai9 mice (Jackson Labs 007909). One week post-administration, mice were perfused with 10% formalin and organs were collected. Necropsied organs were further fixed in 10% formalin at 4 °C overnight. Organs were washed in PBS, transferred to 30% w/v sucrose-PBS overnight, then frozen in OCT (Tissue-Tek). Tissues were cryosectioned into 10 um slices, then stained using conventional protocols. Briefly, tissues were rehydrated in PBS. For troponin T staining, tissues were washed in PBS with 0.2% Tween 20 for 1 hr at RT and permeabilized in 0.5% Triton-X for 15 minutes, then blocked with 5% BSA, 10% goat serum, and 0.5% Triton-X in PBS for 2 hr at RT. Other tissues were blocked with 2% BSA, 5% goat serum, and 1% Triton-X in PBS for 1 hr at RT. Primary antibody incubations were done in blocking buffer overnight at 4 °C. The following primary antibodies and dilutions were used: 1:200 CD31 (BD 553370), 1:200 troponin T (BD

565744). Where applicable, secondary antibodies (Jackson Labs) were applied and cells were counterstained with 10 μg/mL Hoechst in 2% BSA in PBS for 30 min to 1 hr at RT. Tissues were washed in PBS with 0.1 to 0.2% Tween 20 and mounted with Fluoromount-G (Southern Biotech). Tissue sections were imaged on a Nikon Eclipse Ti2 microscope with a Hamamatsu Orca-Flash 4.0 digital camera. Images of each organ type were collected using the same exposure and intensity settings for direct comparison. For unbiased quantification of number of tdTomato cells per area and percent CD31 positive cells, whole slice scans of the heart and lung were acquired from three animals and analyzed using QuPath v0.6.0 software.

Supplementary Material

Refer to Web version on PubMed Central for supplementary material.

ACKNOWLEDGEMENTS

This work was supported by the NIH NIAID (2R01AI132413) and NIH NINDS (DP2 NS111507). KFM was supported by a training grant from the National Heart, Lung, and Blood Institute of the National Institutes of Health (Number 1 T32 HL 160507-1 A1). The authors acknowledge the use of facilities and instrumentation supported by NSF through the UC San Diego Materials Research Science and Engineering Center (UCSD MRSEC), grant # DMR-2011924. Experiments were performed in part at the San Diego Nanotechnology Infrastructure (SDNI) of UCSD, a member of the National Nanotechnology Coordinated Infrastructure, which is supported by the National Science Foundation (Grant ECCS-2025752). The content is solely the responsibility of the authors and does not necessarily represent the official views of the National Institutes of Health. We would also like to thank Bernice Lozada for help with LNP preparation and *in vitro* experiments and Yazmin Hernandez for her help with performing the *in vivo* experiments.

DATA AVAILABILITY STATEMENT

Data needed to evaluate the conclusions in the paper are present in the paper and/or the supplemental data. Additional data are available from authors upon request.

REFERENCES

(1). Hald Albertsen C; Kulkarni JA; Witzigmann D; Lind M; Petersson K; Simonsen JB The Role of Lipid Components in Lipid Nanoparticles for Vaccines and Gene Therapy. Adv. Drug Deliv. Rev. 2022, 188, 114416. 10.1016/j.addr.2022.114416. [PubMed: 35787388]

(2). Kim Y-K RNA Therapy: Rich History, Various Applications and Unlimited Future Prospects. Exp. Mol. Med. 2022, 54 (4), 455–465. 10.1038/s12276-022-00757-5. [PubMed: 35440755]

(3). Kazemian P; Yu S-Y; Thomson SB; Birkenshaw A; Leavitt BR; Ross CJD Lipid-Nanoparticle-Based Delivery of CRISPR/Cas9 Genome-Editing Components. Mol. Pharm. 2022, 19 (6), 1669–1686. 10.1021/acs.molpharmaceut.1c00916. [PubMed: 35594500]

(4). Haque Md. A.; Shrestha A; Mikelis CM; Mattheolabakis G Comprehensive Analysis of Lipid Nanoparticle Formulation and Preparation for RNA Delivery. Int. J. Pharm. X 2024, 8, 100283. 10.1016/j.ijpx.2024.100283. [PubMed: 39309631]

(5). Verma M; Ozer I; Xie W; Gallagher R; Teixeira A; Choy M The Landscape for Lipid-Nanoparticle-Based Genomic Medicines. Nat. Rev. Drug Discov. 2023, 22 (5), 349–350. 10.1038/d41573-023-00002-2. [PubMed: 36627441]

(6). Dilliard SA; Siegwart DJ Passive, Active and Endogenous Organ-Targeted Lipid and Polymer Nanoparticles for Delivery of Genetic Drugs. Nat. Rev. Mater. 2023, 8 (4), 282–300. 10.1038/s41578-022-00529-7. [PubMed: 36691401]

(7). Chen S; Tam YYC; Lin PJC; Sung MMH; Tam YK; Cullis PR Influence of Particle Size on the in Vivo Potency of Lipid Nanoparticle Formulations of siRNA. J. Controlled Release 2016, 235, 236–244. 10.1016/j.jconrel.2016.05.059.

(8). Di J; Du Z; Wu K; Jin S; Wang X; Li T; Xu Y Biodistribution and Non-Linear Gene Expression of mRNA LNPs Affected by Delivery Route and Particle Size. Pharm. Res. 2022, 39 (1), 105–114. 10.1007/s11095-022-03166-5. [PubMed: 35080707]

(9). Dilliard SA; Cheng Q; Siegwart DJ On the Mechanism of Tissue-Specific mRNA Delivery by Selective Organ Targeting Nanoparticles. Proc. Natl. Acad. Sci. 2021, 118 (52), e2109256118. 10.1073/pnas.2109256118. [PubMed: 34933999]

(10). Cheng Q; Wei T; Farbiak L; Johnson LT; Dilliard SA; Siegwart DJ Selective Organ Targeting (SORT) Nanoparticles for Tissue-Specific mRNA Delivery and CRISPR–Cas Gene Editing. Nat. Nanotechnol. 2020, 15 (4), 313–320. 10.1038/s41565-020-0669-6. [PubMed: 32251383]

(11). Tombácz I; Laczkó D; Shahnawaz H; Muramatsu H; Natesan A; Yadegari A; Papp TE; Alameh M-G; Shuvaev V; Mui BL; Tam YK; Muzykantov V; Pardi N; Weissman D; Parhiz H Highly Efficient CD4+ T Cell Targeting and Genetic Recombination Using Engineered CD4+ Cell-Homing mRNA-LNPs. Mol. Ther. 2021, 29 (11), 3293–3304. 10.1016/j.ymthe.2021.06.004. [PubMed: 34091054]

(12). Rurik JG; Tombácz I; Yadegari A; Méndez Fernández PO; Shewale SV; Li L; Kimura T; Soliman OY; Papp TE; Tam YK; Mui BL; Albelda SM; Puré E; June CH; Aghajanian H; Weissman D; Parhiz H; Epstein JA CAR T Cells Produced in Vivo to Treat Cardiac Injury. Science 2022, 375 (6576), 91–96. 10.1126/science.abm0594. [PubMed: 34990237]

(13). Sakurai Y; Abe N; Yoshikawa K; Oyama R; Ogasawara S; Murata T; Nakai Y; Tange K; Tanaka H; Akita H Targeted Delivery of Lipid Nanoparticle to Lymphatic Endothelial Cells via Anti-Podoplanin Antibody. J. Controlled Release 2022, 349, 379–387. 10.1016/j.jconrel.2022.06.052.

(14). Parhiz H; Shuvaev VV; Pardi N; Khoshnejad M; Kiseleva RY; Brenner JS; Uhler T; Tuyishime S; Mui BL; Tam YK; Madden TD; Hope MJ; Weissman D; Muzykantov VR PECAM-1 Directed Re-Targeting of Exogenous mRNA Providing Two Orders of Magnitude Enhancement of Vascular Delivery and Expression in Lungs Independent of Apolipoprotein E-Mediated Uptake. J. Controlled Release 2018, 291, 106–115. 10.1016/j.jconrel.2018.10.015.

(15). Todaro B; Ottalagana E; Luin S; Santi M Targeting Peptides: The New Generation of Targeted Drug Delivery Systems. Pharmaceutics 2023, 15 (6), 1648. 10.3390/pharmaceutics15061648. [PubMed: 37376097]

(16). Ruoslahti E Peptides as Targeting Elements and Tissue Penetration Devices for Nanoparticles. Adv. Mater. 2012, 24 (28), 3747–3756. 10.1002/adma.201200454. [PubMed: 22550056]

(17). Swart LE; Fens MHAM; Van Oort A; Waranecki P; Mata Casimiro LD; Tuk D; Hendriksen M; Van Den Brink L; Schweighart E; Seinen C; Nelson R; Krippner-Heidenreich A; O'Toole T; Schiffelers RM; Kooijmans S; Heidenreich O Increased Bone Marrow Uptake and Accumulation of Very-Late Antigen-4 Targeted Lipid Nanoparticles. Pharmaceutics 2023, 15 (6), 1603. 10.3390/pharmaceutics15061603. [PubMed: 37376052]

(18). Herrera-Barrera M; Ryals RC; Gautam M; Jozic A; Landry M; Korzun T; Gupta M; Acosta C; Stoddard J; Reynaga R; Tschetter W; Jacomino N; Taratula O; Sun C; Lauer AK; Neuringer M; Sahay G Peptide-Guided Lipid Nanoparticles Deliver mRNA to the Neural Retina of Rodents and Nonhuman Primates. Sci. Adv. 2023, 9 (2), eadd4623. 10.1126/sciadv.add4623. [PubMed: 36630502]

(19). Zhang J; Shen H; Xu J; Liu L; Tan J; Li M; Xu N; Luo S; Wang J; Yang F; Tang J; Li Q; Wang Y; Yu L; Yan Z Liver-Targeted siRNA Lipid Nanoparticles Treat Hepatic Cirrhosis by Dual Antifibrotic and Anti-Inflammatory Activities. ACS Nano 2020, 14 (5), 6305–6322. 10.1021/acsnano.0c02633. [PubMed: 32378877]

(20). Soto MR; Lewis MM; Leal J; Pan Y; Mohanty RP; Veyssi A; Maier EY; Heiser BJ; Ghosh D Discovery of Peptides for Ligand-Mediated Delivery of mRNA Lipid Nanoparticles to Cystic Fibrosis Lung Epithelia. Mol. Ther. - Nucleic Acids 2024, 35 (4), 102375. 10.1016/j.omtn.2024.102375. [PubMed: 39640013]

(21). Qin J; Xue L; Gong N; Zhang H; Shepherd SJ; Haley RM; Swingle KL; Mitchell MJ RGD Peptide-Based Lipids for Targeted mRNA Delivery and Gene Editing Applications. RSC Adv. 2022, 12 (39), 25397–25404. 10.1039/D2RA02771B. [PubMed: 36199352]

(22). Swart LE; Koekman CA; Seinen CW; Issa. H; Rasouli. M; Schiffelers RM; Heidenreich O A Robust Post-Insertion Method for the Preparation of Targeted siRNA LNPs. Int. J. Pharm. 2022, 620, 121741. 10.1016/j.ijpharm.2022.121741. [PubMed: 35421533]

(23). Javid H; Oryani MA; Rezagholinejad N; Esparham A; Tajaldini M; Karimi-Shahri M RGD Peptide in Cancer Targeting: Benefits, Challenges, Solutions, and Possible integrin–RGD Interactions. Cancer Med. 2024, 13 (2), e6800. 10.1002/cam4.6800. [PubMed: 38349028]

(24). Hu Q; Gao X; Kang T; Feng X; Jiang D; Tu Y; Song Q; Yao L; Jiang X; Chen H; Chen J CGKRK-Modified Nanoparticles for Dual-Targeting Drug Delivery to Tumor Cells and Angiogenic Blood Vessels. Biomaterials 2013, 34 (37), 9496–9508. 10.1016/j.biomaterials.2013.09.001. [PubMed: 24054848]

(25). Kelly KA; Nahrendorf M; Yu AM; Reynolds F; Weissleder R In Vivo Phage Display Selection Yields Atherosclerotic Plaque Targeted Peptides for Imaging. Mol. Imaging Biol. 2006, 8 (4), 201–207. 10.1007/s11307-006-0043-6. [PubMed: 16791746]

(26). Distasio N; Salmon H; Dierick F; Ebrahimian T; Tabrizian M; Lehoux S VCAM-1-Targeted Gene Delivery Nanoparticles Localize to Inflamed Endothelial Cells and Atherosclerotic Plaques. Adv. Ther. 2021, 4 (2), 2000196. 10.1002/adtp.202000196.

(27). Kheirolomoom A; Kim CW; Seo JW; Kumar S; Son DJ; Gagnon MKJ; Ingham ES; Ferrara KW; Jo H Multifunctional Nanoparticles Facilitate Molecular Targeting and miRNA Delivery to Inhibit Atherosclerosis in ApoE –/– Mice. ACS Nano 2015, 9 (9), 8885–8897. 10.1021/acsnano.5b02611. [PubMed: 26308181]

(28). Son S; Hwang DW; Singha K; Jeong JH; Park TG; Lee DS; Kim WJ RVG Peptide Tethered Bioreducible Polyethylenimine for Gene Delivery to Brain. J. Controlled Release 2011, 155 (1), 18–25. 10.1016/j.jconrel.2010.08.011.

(29). Kumar P; Wu H; McBride JL; Jung K-E; Hee Kim M; Davidson BL; Kyung Lee S; Shankar P; Manjunath N Transvascular Delivery of Small Interfering RNA to the Central Nervous System. Nature 2007, 448 (7149), 39–43. 10.1038/nature05901. [PubMed: 17572664]

(30). Chander N; Basha G; Yan Cheng MH; Witzigmann D; Cullis PR Lipid Nanoparticle mRNA Systems Containing High Levels of Sphingomyelin Engender Higher Protein Expression in Hepatic and Extra-Hepatic Tissues. Mol. Ther. - Methods Clin. Dev. 2023, 30, 235–245. 10.1016/j.omtm.2023.06.005. [PubMed: 37564393]

(31). Belliveau NM; Huft J; Lin PJ; Chen S; Leung AK; Leaver TJ; Wild AW; Lee JB; Taylor RJ; Tam YK; Hansen CL; Cullis PR Microfluidic Synthesis of Highly Potent Limit-Size Lipid Nanoparticles for In Vivo Delivery of siRNA. Mol. Ther. - Nucleic Acids 2012, 1, e37. 10.1038/mtna.2012.28. [PubMed: 23344179]

(32). Waggoner LE; Miyasaki KF; Kwon EJ Analysis of PEG-Lipid Anchor Length on Lipid Nanoparticle Pharmacokinetics and Activity in a Mouse Model of Traumatic Brain Injury. Biomater. Sci. 2023, 10.1039.D2BM01846B. 10.1039/D2BM01846B.

(33). Mo Y; Keszei AFA; Kothari S; Liu H; Pan A; Kim P; Bu J; Kamanzi A; Dai DL; Mazhab-Jafari MT; Chen J; Leslie S; Zheng G Lipid-siRNA Organization Modulates the Intracellular Dynamics of Lipid Nanoparticles. J. Am. Chem. Soc. 2025, 147 (12), 10430–10445. 10.1021/jacs.4c18308. [PubMed: 40068204]

(34). Danhier F; Le Breton A; Préat V RGD-Based Strategies To Target Alpha(v) Beta(3) Integrin in Cancer Therapy and Diagnosis. Mol. Pharm. 2012, 9 (11), 2961–2973. 10.1021/mp3002733. [PubMed: 22967287]

(35). Ward PA Inflammation and $\alpha_v\beta_3$ Integrin. Am. J. Respir. Crit. Care Med. 2012, 185 (1), 5–6. 10.1164/rccm.201110-1859ED. [PubMed: 22210783]

(36). Ludwig BS; Kessler H; Kossatz S; Reuning U RGD-Binding Integrins Revisited: How Recently Discovered Functions and Novel Synthetic Ligands (Re-)Shape an Ever-Evolving Field. Cancers 2021, 13 (7), 1711. 10.3390/cancers13071711. [PubMed: 33916607]

(37). Liu S Radiolabeled Cyclic RGD Peptide Bioconjugates as Radiotracers Targeting Multiple Integrins. Bioconjug. Chem. 2015, 26 (8), 1413–1438. 10.1021/acs.bioconjchem.5b00327. [PubMed: 26193072]

(38). Kim J; Hong S-Y; Park H; Kim D-S; Lee W Structure and Function of RGD Peptides Derived from Disintegrin Proteins. Mol. Cells 2005, 19 (2), 205–211. 10.1016/S1016-8478(23)13157-8. [PubMed: 15879703]

(39). Li N; Qiu S; Fang Y; Wu J; Li Q Comparison of Linear vs. Cyclic RGD Pentapeptide Interactions with Integrin Avβ3 by Molecular Dynamics Simulations. Biology 2021, 10 (7), 688. 10.3390/biology10070688. [PubMed: 34356543]

(40). Huang G; Zhou Z; Srinivasan R; Penn MS; Kottke-Marchant K; Marchant RE; Gupta AS Affinity Manipulation of Surface-Conjugated RGD Peptide to Modulate Binding of Liposomes to Activated Platelets. Biomaterials 2008, 29 (11), 1676–1685. 10.1016/j.biomaterials.2007.12.015. [PubMed: 18192005]

(41). Han EL; Tang S; Kim D; Murray AM; Swingle KL; Hamilton AG; Mrksich K; Padilla MS; Palanki R; Li JJ; Mitchell MJ Peptide-Functionalized Lipid Nanoparticles for Targeted Systemic mRNA Delivery to the Brain. Nano Lett. 2025, 25 (2), 800–810. 10.1021/acs.nanolett.4c05186. [PubMed: 39688915]

(42). Liu Y; Bajjuri KM; Liu C; Sinha SC Targeting Cell Surface Alpha(v)Beta(3) Integrin Increases Therapeutic Efficacies of a Legumain Protease-Activated Auristatin Prodrug. Mol. Pharm. 2012, 9 (1), 168–175. 10.1021/mp200434n. [PubMed: 22044266]

(43). Bankhead P; Loughrey MB; Fernández JA; Dombrowski Y; McArt DG; Dunne PD; McQuaid S; Gray RT; Murray LJ; Coleman HG; James JA; Salto-Tellez M; Hamilton PW QuPath: Open Source Software for Digital Pathology Image Analysis. Sci. Rep. 2017, 7 (1), 16878. 10.1038/s41598-017-17204-5. [PubMed: 29203879]

(44). Mui BL; Tam YK; Jayaraman M; Ansell SM; Du X; Tam YYC; Lin PJ; Chen S; Narayanannair JK; Rajeev KG; Manoharan M; Akinc A; Maier MA; Cullis P; Madden TD; Hope MJ Influence of Polyethylene Glycol Lipid Desorption Rates on Pharmacokinetics and Pharmacodynamics of siRNA Lipid Nanoparticles. Mol. Ther. - Nucleic Acids 2013, 2, e139. 10.1038/mtna.2013.66. [PubMed: 24345865]

(45). Holig P; Bach M; Volkel T; Nahde T; Hoffmann S; Muller R; Kontermann RE Novel RGD Lipopeptides for the Targeting of Liposomes to Integrin-Expressing Endothelial and Melanoma Cells. Protein Eng. Des. Sel. 2004, 17 (5), 433–441. 10.1093/protein/gzh055. [PubMed: 15235124]

(46). Madisen L; Zwingman TA; Sunkin SM; Oh SW; Zariwala HA; Gu H; Ng LL; Palmiter RD; Hawrylycz MJ; Jones AR; Lein ES; Zeng H A Robust and High-Throughput Cre Reporting and Characterization System for the Whole Mouse Brain. Nat. Neurosci. 2010, 13 (1), 133–140. 10.1038/nn.2467. [PubMed: 20023653]

(47). Singh B; Rawlings N; Kaur A Expression of Integrin Avβ3 in Pig, Dog and Cattle. Histol. Histopathol. 2001, No. 16, 1037–1046. 10.14670/HH-16.1037. [PubMed: 11642723]

(48). Schiffelers R Anti-Tumor Efficacy of Tumor Vasculature-Targeted Liposomal Doxorubicin. J. Controlled Release 2003, 91 (1–2), 115–122. 10.1016/S0168-3659(03)00240-2.

(49). Cheng MHY; Leung J; Zhang Y; Strong C; Basha G; Momeni A; Chen Y; Jan E; Abdolahzadeh A; Wang X; Kulkarni JA; Witzigmann D; Cullis PR Induction of Bleb Structures in Lipid Nanoparticle Formulations of mRNA Leads to Improved Transfection Potency. Adv. Mater. 2023, 35 (31), 2303370. 10.1002/adma.202303370.

(50). Parhiz H; Shuvaev VV; Li Q; Papp TE; Akyianu AA; Shi R; Yadegari A; Shahnawaz H; Semple SC; Mui BL; Weissman D; Muzykantov VR; Glassman PM Physiologically Based Modeling of LNP-Mediated Delivery of mRNA in the Vascular System. Mol. Ther. - Nucleic Acids 2024, 35 (2), 102175. 10.1016/j.omtn.2024.102175. [PubMed: 38576454]

(51). Schindelin J; Arganda-Carreras I; Frise E; Kaynig V; Longair M; Pietzsch T; Preibisch S; Rueden C; Saalfeld S; Schmid B; Tinevez J-Y; White DJ; Hartenstein V; Eliceiri K; Tomancak P; Cardona A Fiji: An Open-Source Platform for Biological-Image Analysis. Nat. Methods 2012, 9 (7), 676–682. 10.1038/nmeth.2019. [PubMed: 22743772]

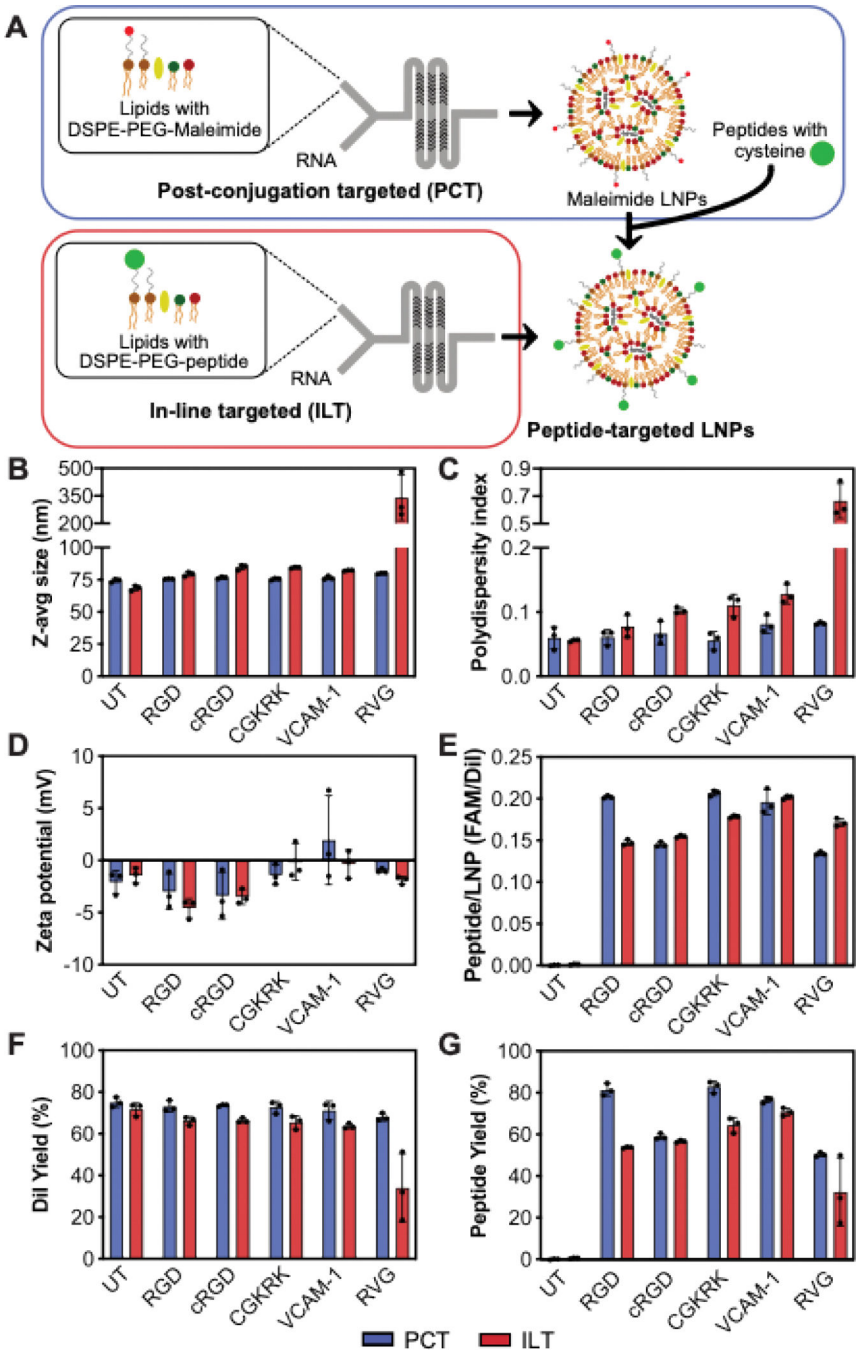

Figure 1. Formulation of peptide targeted LNPs through in-line or post-modification with five different peptide ligands

(A) Schematic of the in-line targeted and post-conjugation targeted formulation methods. (B) Hydrodynamic diameters, (C) polydispersity indices, (D) zeta potentials, (E) absorbance ratios of FAM-labeled peptides and DiI on LNPs. (F) Yield of LNPs calculated by absorbance of DiI and (G) yield of targeting peptides calculated by absorbance of FAM.

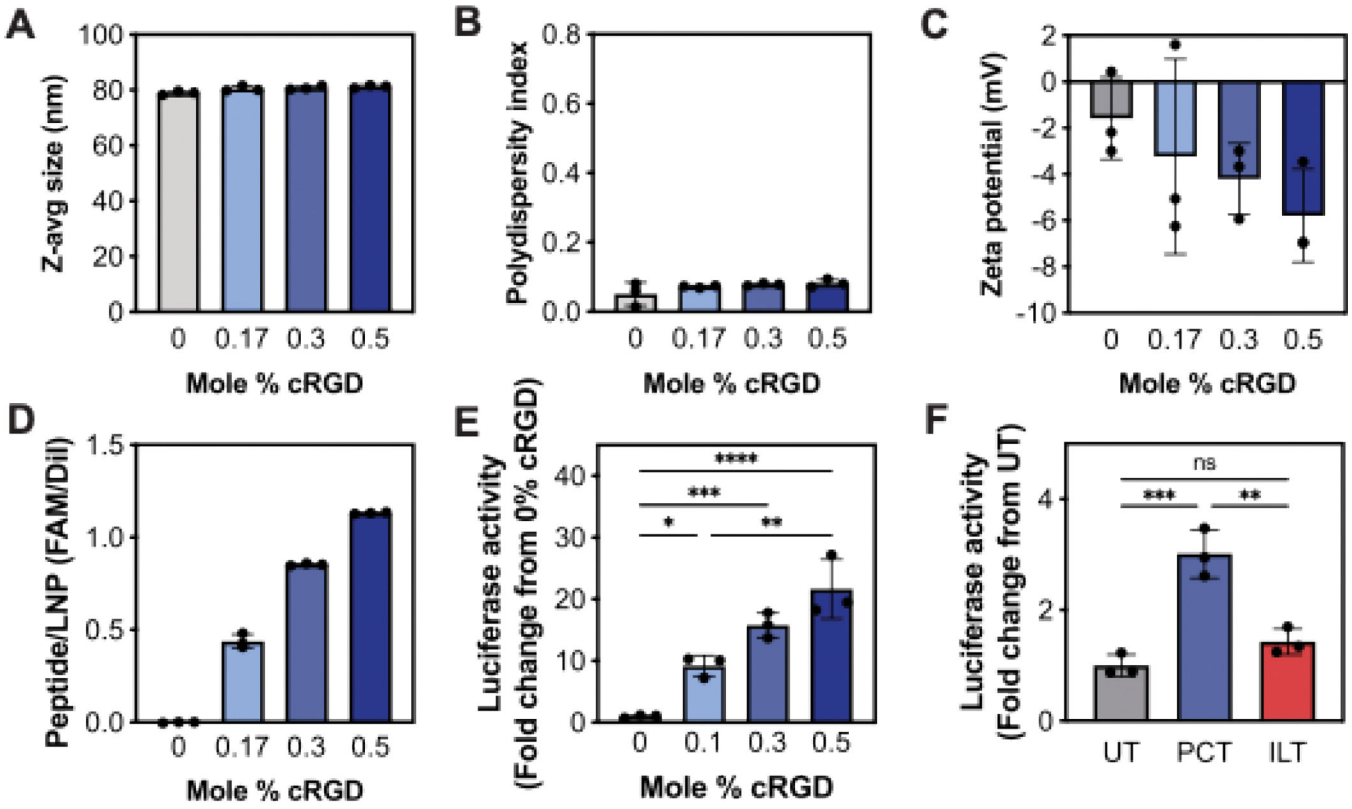

Figure 2. Activity of peptide LNPs created through inline or post-modification

PCT LNPs were formulated with 1 mole% DSPE-PEG-maleimide and conjugated with varying amounts of cRGD peptide. (A) Hydrodynamic diameters, (B) polydispersity indices, (C) zeta potentials, and (D) absorbance ratios of FAM-labeled peptides and DiI. (E) LNPs were formulated with FLuc mRNA and transfection efficiency of LNPs was measured in MDA-MB-435 cells 72 hours after treatment. (F) Transfection efficiency of PCT and ILT LNPs with 0.5 mole% cRGD compared to untargeted LNPs (UT). (n=3, mean ± SD; One-way ANOVA with Tukey's post-test, *$p < 0.05$, **$p < 0.01$, ***$p < 0.001$, ****$p < 0.0001$.)

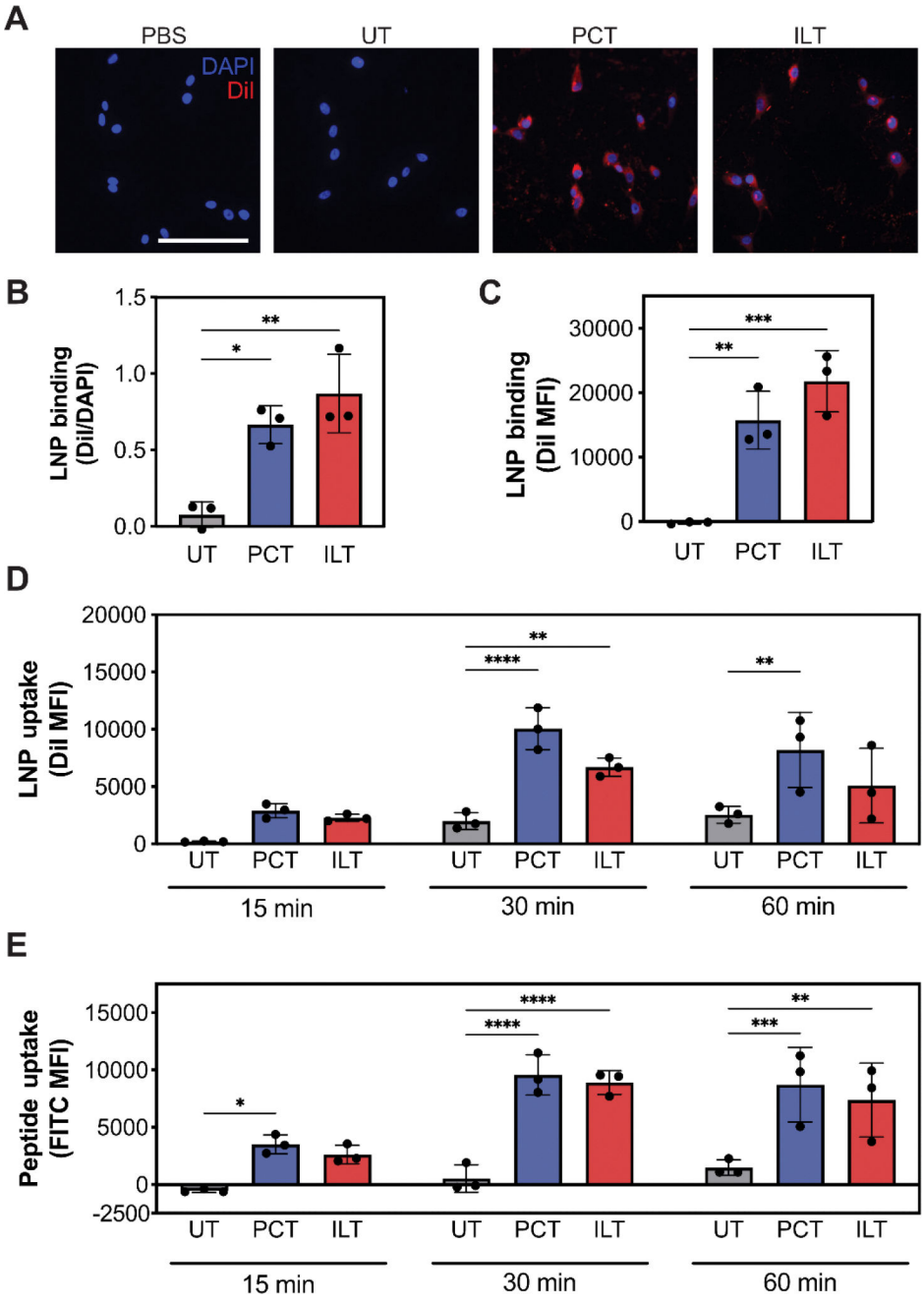

Figure 3. Binding and uptake of ILT and PCT cRGD LNPs

(A) Imaging and (B) quantification of DiI-labeled untargeted and cRGD-targeted LNPs binding to MDA-MB-435 cells after 3 hours of incubation at 4 °C (blue, DAPI; red, DiI. Scale bar = 100 μm). (C) Quantification of LNP binding by flow cytometry after 3 hours of incubation at 4 °C (MFI = median fluorescence intensity). Quantification of LNP uptake in cells by flow cytometry after incubation at 37°C, measured by (D) DiI and (E) FITC-labeled peptide MFI. (n = 3, mean ± SD; one-way ANOVA with Tukey's post-test, *$p < 0.05$, **$p < 0.01$, ***$p < 0.001$, ****$p < 0.0001$.)

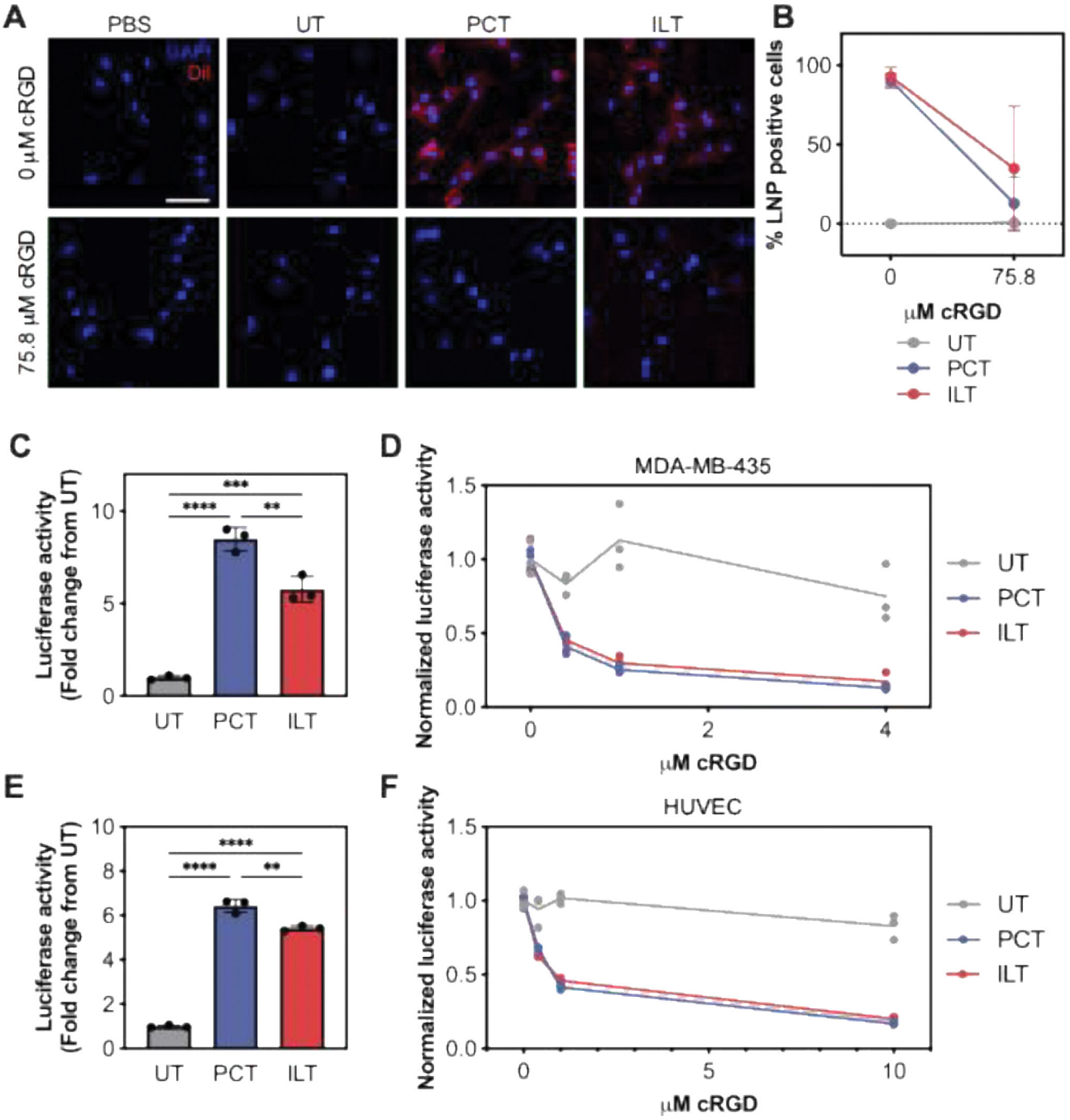

Figure 4. Binding and transfection of cRGD targeted LNPs is ligand specific.

(A) Imaging and (B) quantification of DiI-labeled untargeted and cRGD-targeted LNPs binding in MDA-MB-435 cells at 4 °C in the absence and presence of free cRGD (blue, DAPI; red, DiI. scale bar = 50 μm). Transfection activity of untargeted, PCT, and ILT cRGD LNPs modified with 0.15 mole% peptide in MDA-MB-435 cells (C) without and (D) with the presence of competing free cRGD peptide. Transfection activity of untargeted, PCT, and ILT cRGD LNPs in HUVECs (E) without and (F) with the prescence of competing free

cRGD peptide (n=3, mean ± SD; One-way ANOVA with Tukey's post-test, *$p < 0.05$, **$p < 0.01$, ***$p < 0.001$, ****$p < 0.0001$).

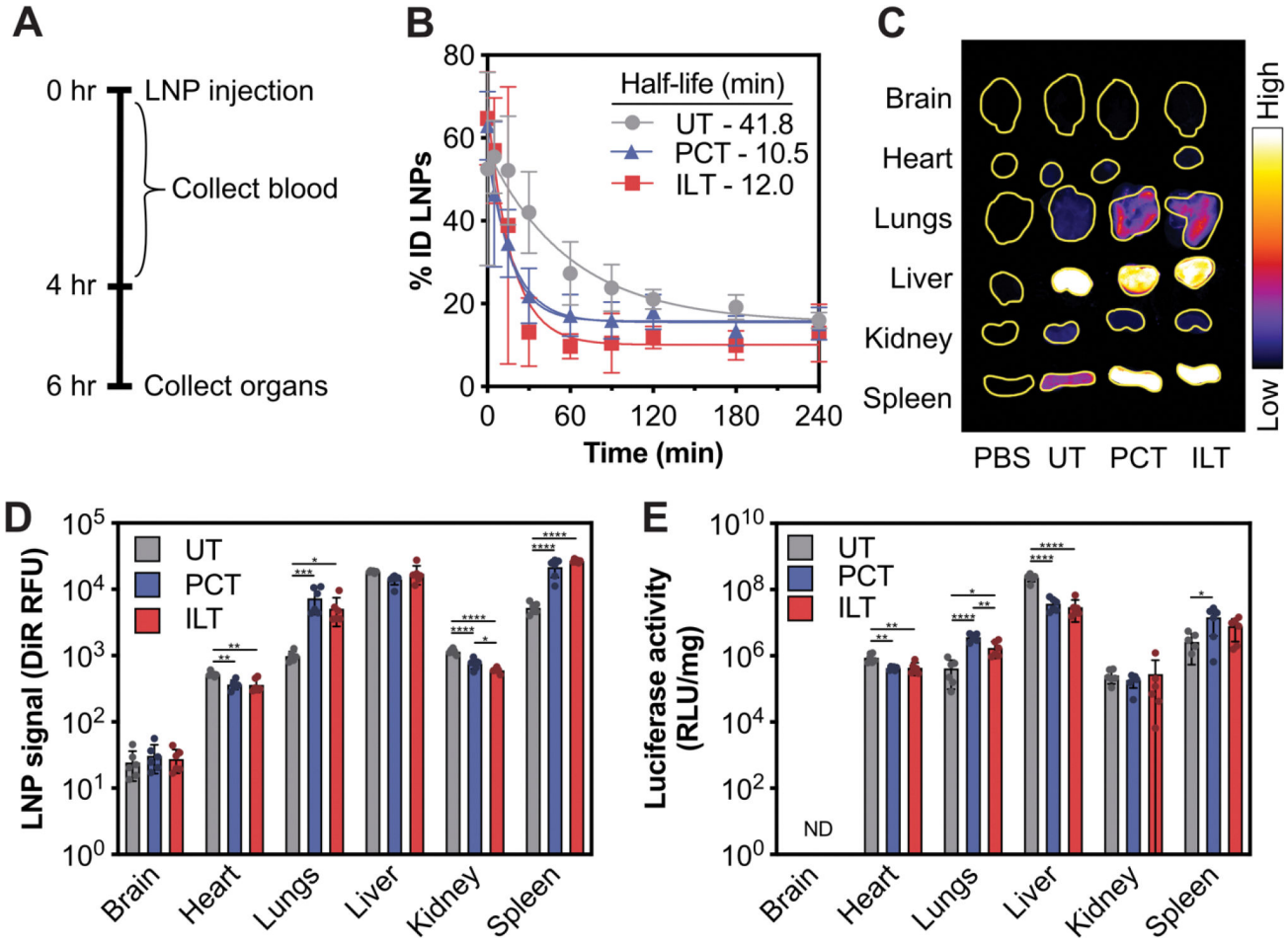

Figure 5. Comparison of pharmacokinetics and activity in healthy mice

(A) Schematic of experiment. (B) Targeted cRGD LNP blood half-life as measured by DiR labeled LNPs. (C) Representative targeted cRGD LNP organ biodistribution and (D) quantification as measured by fluorescence surface imaging of DiR labeled LNPs. (E) Transfection of targeted cRGD LNPs. (n=6, mean ± SD; one-way ANOVA with Tukey's post-test within each organ type, *$p < 0.05$, **p < 0.01, ***$p < 0.001$, ****$p < 0.0001$; ND not detected.)

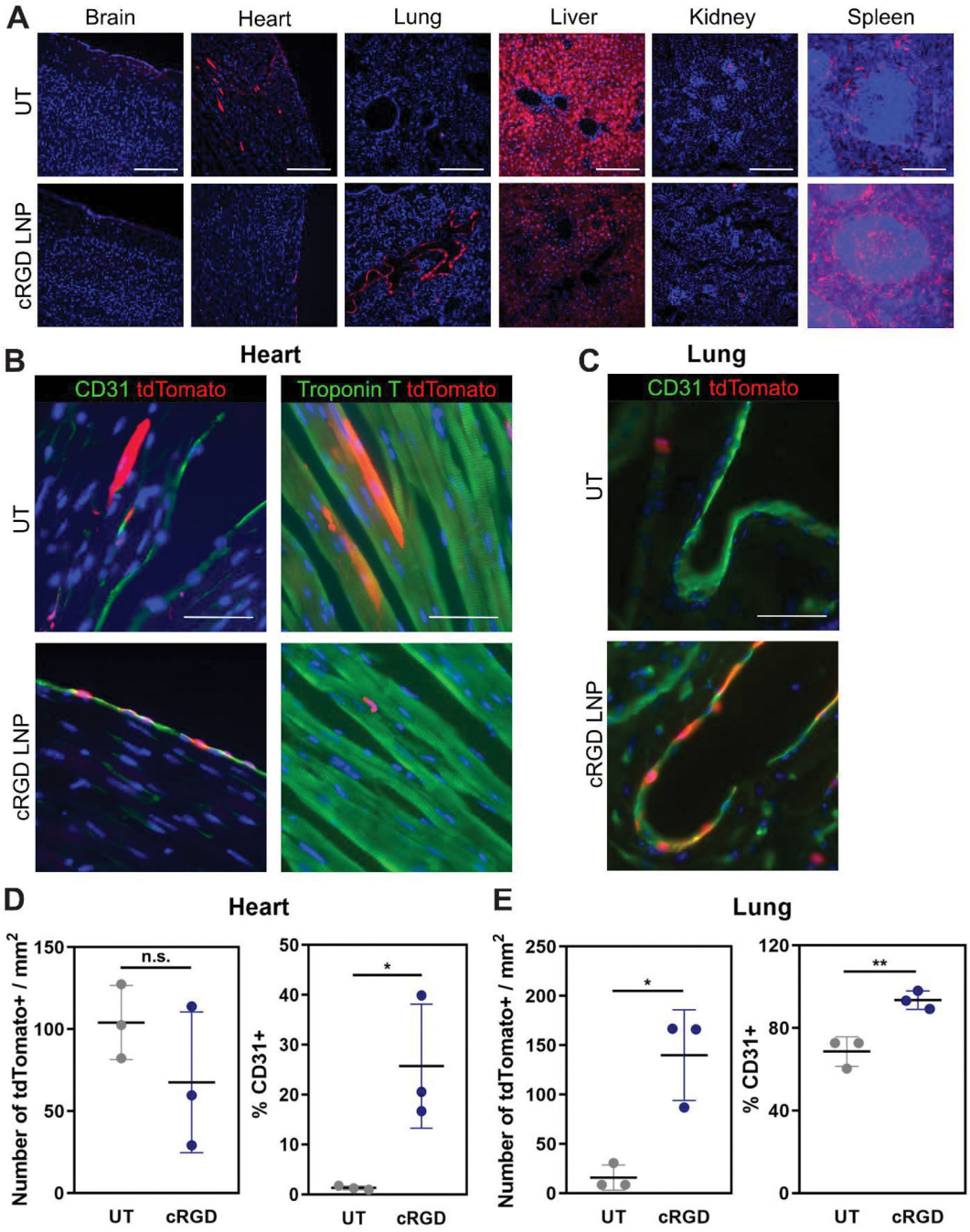

Figure 6. Cell tropism of cRGD PCT LNPs

(A) Reporter transgene expression in the heart, lung, spleen, liver, and kidney in Ai9 mice systemically administered untargeted and cRGD targeted LNPs carrying Cre recombinase mRNA (blue, DAPI; red, tdTomato, scale bar = 200 μm). (B) Reporter transgene expression and CD31 or troponin T staining (green) in heart (scale bar = 50 μm). (C) Reporter transgene expression and CD31 staining (green) in lung (scale bar = 50 μm; n=3, representative images). Quantification of number of tdTomato$^+$ cells/mm^2 and percent of tdTomato$^+$ cells

that were $CD31^+$ in analysis of whole organ slices of the (D) heart and (E) lungs (n=3, *p<0.05, **p<0.01, Welch test).

Table 1. Peptides used in formulations.

FAM, carboxyfluorescein; Ahx, aminohexanoic acid.

Peptide	Sequence	Residue Charges	Length (AA)	MW (Da)	GRAVY
RGD	(FAM)Ahx-CRGD	+1, −1	4	920.96	−1.48
cRGD	CG(K-FAM)CRGDC └S-S┘	+1, −1	8	1197.3	−0.68
CGKRK	(FAM)CGKRK	+3	5	949.06	−2.04
VCAM-1	VHPKQHRGGS(K-FAM)GC	+2	13	1747.2	−1.27
RVG	C(K-FAM)YTIWMPENPRPGTP CDIFTNSRGKRASNG	+4, −2	31	3856.3	−0.93